Multiple Andreev Reflections in a Carbon Nanotube Quantum Dot

M. R. Buitelaar,* W. Belzig, T. Nussbaumer, B. Babić, C. Bruder, and C. Schönenberger
Institut für Physik, Universität Basel, Klingelbergstrasse 82, CH-4056 Basel, Switzerland
(Received 9 April 2003; published 1 August 2003)

We report resonant multiple Andreev reflections in a multiwall carbon nanotube quantum dot coupled to superconducting leads. The position and magnitude of the subharmonic gap structure is found to depend strongly on the level positions of the single-electron states which are adjusted with a gate electrode. We discuss a theoretical model of the device and compare the calculated differential conductance with the experimental data.

DOI: 10.1103/PhysRevLett.91.057005 PACS numbers: 74.45.+c, 73.23.Hk, 73.63.Fg, 73.63.Kv

The electronic transport properties of quantum dots coupled to metallic leads have been the object of extensive theoretical and experimental study [1]. When weakly coupled to its leads, the low-temperature transport characteristics are dominated by size and charge quantization effects, parametrized by the single-electron level spacing ΔE and charging energy U_C. When the coupling is increased, higher-order tunneling processes such as the Kondo effect become important [2]. New effects are expected when the leads coupled to the quantum dot are superconductors. In that case, electron transport is mediated by multiple Andreev reflection (MAR) [3,4]. Unlike conventional *S-N-S* devices, however, the MAR structure is now expected to strongly depend on the level positions which can be tuned with a gate electrode [5,6]. The influence of Coulomb and Kondo correlations have been addressed theoretically in Ref. [7].

Because MAR is suppressed rapidly for low-transparency junctions, its observation requires a relatively strong coupling between the leads and quantum dot — even more so as on-site Coulomb repulsion, which is common to weakly coupled dots, is expected to reduce Andreev processes even further. In the experiments of Ralph *et al.*, the transport was indeed dominated by charging effects and MAR was completely suppressed [8].

The coupling to the leads, expressed in the lifetime broadening Γ of the quantum dot levels, should be compared to the superconducting gap energy Δ. Favorable for the observation of MAR in a quantum dot are coupling strengths of the order of $\Gamma \sim \Delta$ and a small charging energy $U_C < \Delta$. Together with the restriction that $\Gamma < \Delta E$ (for any quantum dot), this leads to the approximate condition $U_C \lesssim \Gamma \lesssim \Delta E$. For most quantum dots, typically the opposite is true and $\Delta E < U_C$. It has recently been shown [9], however, that well-coupled multiwall carbon nanotube (MWNT) quantum dots can have favorable ratios of $\Delta E/U_C \sim 2$, and U_C can be as small as 0.4 meV, comparable to the energy gap 2Δ of a conventional superconductor such as Al.

Here we report on the experimental study of resonant MAR in a MWNT quantum dot. The superconducting leads to the MWNT consist of a Au/Al bilayer (45/135 nm) deposited on top of the nanotube [see Fig. 1(d)]. Before investigating the system in the superconducting state, the sample is first characterized in the normal state by applying a small magnetic field. From these measurements, relevant parameters such as ΔE, U_C, and Γ are obtained. We then discuss a theoretical model that describes the differential conductance of an individual level in a quantum dot coupled to superconducting electrodes. In the final part of the paper, we compare the calculated differential conductance with the experimental data.

Figure 1 shows a gray scale representation of the differential conductance dI/dV_{sd} versus source drain (V_{sd}) and gate voltage (V_g) at $T = 50$ mK when the contacts are driven normal by a small magnetic field. The dotted white lines outline the onset of first-order tunneling and appear when a discrete energy level of the quantum dot is at resonance with the electrochemical potential of one of the leads. From these and other electron states measured

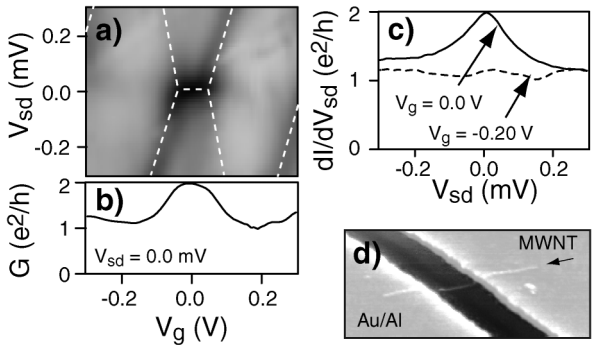

FIG. 1. (a) Gray scale representation of the differential conductance dI/dV_{sd} as a function of source drain (V_{sd}) and gate voltage (V_g) at $T = 50$ mK and $B = 26$ mT for a MWNT quantum dot (darker = more conductive). (b) Linear-response conductance $G(V_g)$. The appearance of a single broad peak is due to the Kondo effect. (c) dI/dV_{sd} at two different values of V_g. (d) Typical device geometry. For the measurements presented here, the electrode spacing is 0.25 μm and the MWNT length 1.5 μm. The Si substrate is used as a gate electrode.

 0031-9007/03/91(5)/057005(4)$20.00

for this sample (about 20 in total), we obtain an average single-electron level spacing $\Delta E \sim 0.6$ meV and a charging energy $U_C \sim 0.4$ meV. Since $U_C = e^2/C_\Sigma$, this yields $C_\Sigma = 400$ aF for the total capacitance which is the sum of the gate capacitance (C_g) and the contact capacitances C_s (source) and C_d (drain). From the data of Fig. 1(a), we obtain $C_g/C_\Sigma = 0.0036$, and $C_s/C_d = 0.45$. The lifetime broadening $\Gamma \sim 0.35$ meV is obtained from the width of the single-electron peaks at finite source-drain voltage taking the background conductance into account.

The high-conductance ridge around $V_{sd} = 0$ mV in Fig. 1(a) is a manifestation of the spin-1/2 Kondo effect occurring when the number of electrons on the dot is odd. As a result, the Coulomb valley in the conductance has disappeared in this region of V_g [see Fig. 1(b)]. The appearance of the Kondo effect is an indication that the coupling to the leads is relatively strong. We will not discuss the Kondo effect here, and instead refer to Ref. [10].

When the magnetic field is switched off, the leads become superconducting. To calculate the expected differential conductance in the superconducting state of the leads, we have used the nonequilibrium Green's function technique [11]. We model the quantum dot as a series of spin-degenerate resonant levels coupled to electrodes, which are assumed to have a BCS spectral density. Note that neither electron-electron interaction (Coulomb blockade) nor exchange correlations (Kondo effect) are accounted for in the model, which may, therefore, not explain all details of the actual measurements. However, the interplay between MAR and resonant scattering already leads to strongly nonlinear IV characteristics and reproduces most of the key features of the data. The main parameters entering the calculation are the two tunneling rates $\Gamma_{s(d)}$ and Δ. In the model, we account for the gate voltage by a shift of the level, which can be adjusted according to the experimentally observed Coulomb diamonds (see Fig. 1).

The discrete nature of the single-electron states is most pronounced when Γ is small. Therefore, before presenting the model calculation that directly compares to the experimental data, we first discuss the transport characteristics of a single spin-degenerate level with a relatively weak and symmetric coupling to the superconducting leads along the lines of Refs. [5,6]. The total tunneling rate $\Gamma \equiv \Gamma_s + \Gamma_d$ is set to Δ. Figure 2 shows the corresponding gray scale representation of the calculated differential conductance dI/dV_{sd} versus $\varphi_g := eV_g C_g/C_\Sigma$ and eV_{sd}. The peak structure in dI/dV_{sd} at $V_{sd} < 2\Delta/e$ is the result of MAR. In general, Andreev channels become available for transport at voltages $V_{sd} = 2\Delta/ne$, where n is an integer number. These positions are indicated by the horizontal dashed black lines in Fig. 2(a). The appearance and magnitude of the MAR peaks, however, is strongly dependent on the position of the resonant level in the quantum dot with respect to the Fermi energy of the leads. Only those MAR trajectories that connect the resonant level to the leads' BCS spectral densities give a significant contribution to the current. Consider, for example, the position marked by C in Fig. 2(a), which corresponds to the schematics of Fig. 2(c) and indicates the position $(\varphi_g, eV_{sd}) = (0, 2\Delta/3)$. The corresponding Andreev trajectory connects the gap edges of the source and drain electrodes and includes the resonant level which is situated exactly in between the respective Fermi energies. This results in the large peak in dI/dV_{sd} seen in Fig. 2(b).

A similar peak is absent at $(\varphi_g, eV_{sd}) = (0, \Delta)$, corresponding to point D in Fig. 2(a). Now, the corresponding trajectories [see Fig. 2(d)] do not directly connect the resonant level to the leads' spectral densities, and therefore do not significantly contribute to the current. Only when the gate voltage is adjusted to align the level with the Fermi energy of one of the leads [indicated by the arrows in Fig. 2(a)] a peak in dI/dV_{sd} is observed. It can be shown (for symmetric junctions) that the subharmonic gap structure at $V_g = 0$ is suppressed for all

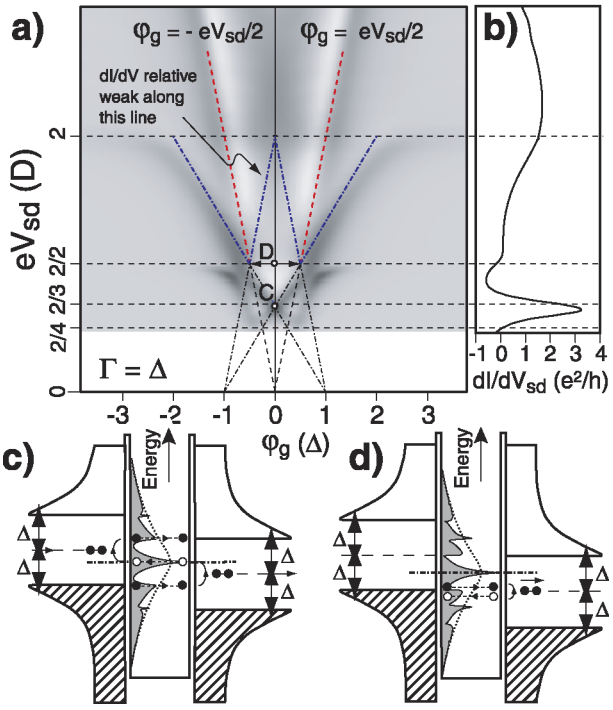

FIG. 2 (color online). (a) Gray scale representation of the calculated differential conductance as a function of V_{sd} and level position ($\varphi_g \propto V_g$) for a single-electron level coupled symmetrically to superconducting electrodes. For clarity, the low-energy part $eV_{sd} \lesssim 2\Delta/4$ has been omitted. The dashed lines indicate resonance positions, as explained in the text. (b) Differential conductance at $\varphi_g = 0$. (c) Single electron state (dash-dotted lines), corresponding to point C in panel (a), between superconducting source and drain electrodes with spectral density (shaded, log scale). The Lorentzian level in the normal state (dotted lines) is replaced by a narrow central resonance accompanied by a series of satellite peaks. (d) Same as (c) for point D in panel (a).

voltages $V_{sd} = 2\Delta/ne$ with $n =$ even [5,6]. When V_{sd} is increased beyond Δ/e, peaks are observed either when the level stays aligned with the electrochemical potential of the leads (dashed lines: $\varphi_g = \pm eV_{sd}/2$) or when the level follows the gap edges as an initial or final state of an Andreev process [dash-dotted lines: $\varphi_g = \pm(\Delta - eV_{sd}/2)$ or $\varphi_g = \pm(\Delta - 3eV_{sd}/2)$].

We now turn to the actual measurements of the differential conductance when the leads are in the superconducting state. Figure 3 shows a gray scale representation of the measured dI/dV_{sd} versus V_{sd} and V_g at $B = 0$ mT for the same single-electron state of Fig. 1. A number of differences between the normal state (Fig. 1) and superconducting state (Fig. 3) can be observed. The horizontal high-conductance lines at $V_{sd} = \pm 0.2$ mV in Fig. 3, for example, are attributed to the onset of quasiparticle tunneling when $V_{sd} = 2\Delta/e$ [12]. The subgap structure at $V_{sd} < 2\Delta/e$ is attributed to MAR. As anticipated, the magnitude and the position (dashed white lines) of MAR peaks depend on V_g. To allow for comparison with theory, the adjustable parameters of the model are set to the values obtained from the measurement of Fig. 1. The most important parameter is the coupling between the electrodes and the dot which turns out to be $\Gamma \sim 3.5\Delta$. The voltage division between the two tunnel barriers separating the quantum dot from the leads is $C_s/C_d = 0.45$. The individual tunneling rates are not exactly known but are not expected to show a strong asymmetry [13]. The neighboring single-electron states, separated by $\Delta E \sim 6.5\Delta$, are included in the calculation, as well as the finite temperature which is set to $T = 0.1\Delta$.

The resulting calculated gray scale representation of the differential conductance is shown in Fig. 4. The overall appearance clearly resembles the measured data of Fig. 3. For example, both the model and the measured data show a large peak in dI/dV_{sd} around $V_{sd} = 0$ mV when the electron state is at resonance with the electrochemical potential of the leads (i.e., at $V_g = 0$). When the level is moved away from this position, the linear-response conductance rapidly decays to values below its normal-state value. In contrast, the differential conductance peak at $V_{sd} = 2\Delta/e$ shows the opposite behavior (both in the model as in the experiment). At $V_g = 0$, this peak is much less pronounced than at lower values of V_g. These observations are similar to conventional S-N-S structures, such as atomic-sized break junctions [14]: For large transparencies of the junction a peak is observed at $V_{sd} = 0$ but no structure at 2Δ, while for small transparencies a gap is observed around $V_{sd} = 0$ and a large peak at 2Δ marks the onset of quasiparticle tunneling. In contrast to break junctions, for which the transparency depends on the atomic arrangement, the effective transparency can be tuned in a quantum dot by moving the level position through the gate electrode. The effective transparency is large if the level is aligned with the Fermi levels of the leads (on resonance) and it is small otherwise (off resonance).

The subharmonic gap structure is clearly visible in the measured data of Fig. 3 and has a similar gate-voltage dependence as in the model calculation of Fig. 4. However, there are several differences. The most dramatic one is the pronounced peak at $(V_g, V_{sd}) = (0, \Delta/e)$ in the measurement [Fig. 3(c)]. Because this position corresponds to an even MAR cycle, it should be absent based on our previous consideration [see Fig. 2(d)].

Let us compare theory and experiment by focusing on the dI/dV_{sd} line traces shown in Figs. 3(b) and 3(c) and

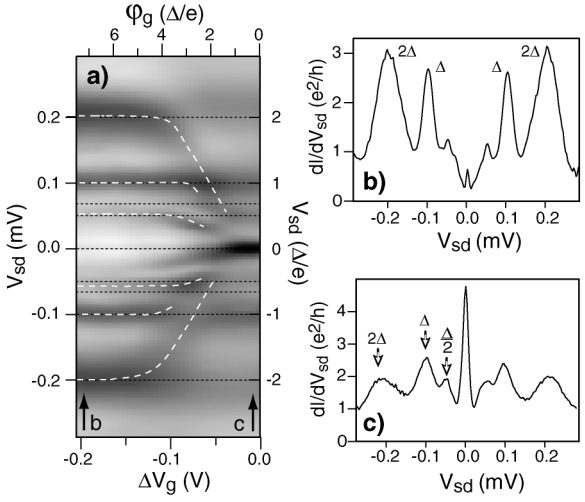

FIG. 3. (a) Gray scale representation of the measured differential conductance as a function of V_{sd} and V_g at $T = 50$ mK with the leads in the superconducting state. The gate voltage range corresponds to the left part of Fig. 1(a). The dashed white lines emphasize the position of the MAR peaks. (b),(c) Differential conductance at the positions given in panel (a).

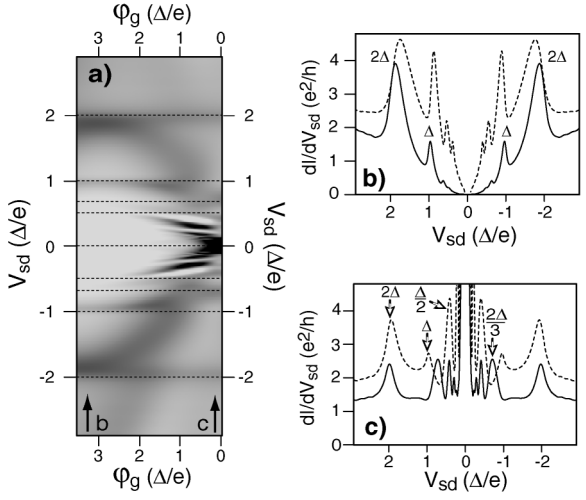

FIG. 4. (a) Gray scale representation of the calculated differential conductance as a function of V_{sd} and level position (φ_g). The different adjustable parameters represent the experimental situation (see text). (b),(c) Differential conductance at the positions given in panel (a). For the two dashed curves, Γ has been chosen approximately twice as large as the experimental value.

Figs. 4(b) and 4(c) (solid curves). In panels (b), the dot level is off resonance, while it is on resonance in panels (c). For the former case, experiment and theory agree fairly well. The differences in MAR structure between model and experiment are much more pronounced at the resonance position. Whereas the experiment [Fig. 3(c)] reveals pronounced peaks at $\Delta/2$, Δ, and 2Δ, the calculated dI/dV_{sd} [Fig. 4(c), solid] reveals fine structure for small V_{sd} and pronounced peaks at $2\Delta/3$ and 2Δ. According to our previous discussion, dI/dV_{sd} should indeed show a pronounced peak at $V_{sd} = 2\Delta/3e$, if the dot level is centered in the middle, i.e., for $\varphi_g = 0$ at point C in Figs. 2(a) and 2(c). It rather appears in the experiment that, contrary to expectations, the subgap feature at $2\Delta/3$ is missing, while the "forbidden" at Δ is present. Such behavior would be expected only for very asymmetric junctions having $C_s/C_d \ll 1$ [15], which is not the case in the present work.

There are different imaginable scenarios that may account for the observed Δ peak and the lack of fine structure around $V_{sd} = 0$ mV in the data of Fig. 3(c). Inelastic scattering processes inside the dot, for example, would broaden and obscure higher-order MAR features. Other possible reasons may be found in a broadened BCS spectral density (the superconductor consists of a bilayer of Au/Al [16]) or a suppression of higher-order MAR due to the on-site Coulomb repulsion.

In a phenomenological approach, we may try to account for the additional broadening by manually introducing larger bare couplings $\Gamma_{s,d}$. Many curves with varying parameters were calculated of which a representative set is displayed in Figs. 4(b) and 4(c) (dashed curves) corresponding to relatively large dot-electrode couplings of $\Gamma_s = 2.5\Delta$ and $\Gamma_d = 3.5\Delta$. For the off-resonance position [Fig. 4(b)], the main effect of the larger Γ is the increased magnitude of dI/dV_{sd}. In contrast, the MAR structures significantly changes for the resonance position [Fig. 4(c)]. Remarkably, at large coupling Γ, peaks now appear at 2Δ, Δ, and $\Delta/2$. These peaks do not originate from the resonant level, but from the two neighboring ones which are off resonance (the dot levels are spaced by $\Delta E \approx 6.5\Delta$). Though the agreement is now reasonable, there is one remaining problem. We were unable to reproduce the relative peak height between the 2Δ and Δ peaks. Using any reasonable set of parameters, the 2Δ peak is always larger than the Δ peak in the model, while it is the opposite in the experiment. We emphasize that the model does not take into account interaction and correlations. Since a Kondo resonance is observed in the normal state, which need not be suppressed in the superconducting state [10], this may be the origin of the discrepancy. The Kondo resonance changes the spectral density in the leads by adding spectral weight to the center of the gap and removing spectral weight from the gap edges. The former tends to enhance the Δ peak, while the latter tends to suppress the 2Δ one. This explanation is attractive, but more work both in theory and experiment is needed to substantiate it.

In conclusion, we have investigated the nonlinear conductance characteristics of a quantum dot coupled to superconducting electrodes. We find a strong dependence of the MAR structure on the level position of the single-electron states. The experimental data is compared with a theoretical model, assuming a BCS density of states in the electrodes and an interaction-free dot. Reasonable agreement is possible, if the tunneling coupling to the leads is enhanced by a factor ~ 2 in the model as compared to the experimental value. There are additional subtle differences which point to the importance of interaction and exchange correlations.

We acknowledge contributions by H. Scharf and M. Iqbal. We thank L. Forró for the MWNT material and J. Gobrecht for providing the oxidized Si substrates. This work has been supported by the Swiss NFS, BBW, and the NCCR on Nanoscience.

*Present address: Cavendish Laboratory, Cambridge, UK.

[1] L. P. Kouwenhoven *et al.*, in *Mesoscopic Electron Transport*, edited by L. L. Sohn, L. P. Kouwenhoven, and G. Schön (Kluwer, Dordrecht, 1997).
[2] L. Kouwenhoven and L. Glazman, Phys. World **14**, 33 (2001).
[3] A. F. Andreev, Sov. Phys. JETP **19**, 1228 (1964).
[4] M. Octavio, M. Tinkham, G. E. Blonder, and T. M. Klapwijk, Phys. Rev. B **27**, 6739 (1983).
[5] A. Levy Yeyati, J. C. Cuevas, A. López-Dávalos, and A. Martín-Rodero, Phys. Rev. B **55**, R6137 (1997).
[6] G. Johansson, E. N. Bratus, V. S. Shumeiko, and G. Wendin, Phys. Rev. B **60**, 1382 (1999).
[7] Y. Avishai, A. Golub, and A. D. Zaikin, Phys. Rev. B **63**, 134515 (2001); Y. Avishai, A. Golub, and A. D. Zaikin, Phys. Rev. B **67**, 041301 (2003).
[8] D. C. Ralph, C. T. Black, and M. Tinkham, Phys. Rev. Lett. **74**, 3241 (1995).
[9] M. R. Buitelaar, A. Bachtold, T. Nussbaumer, M. Iqbal, and C. Schönenberger, Phys. Rev. Lett. **88**, 156801 (2002).
[10] M. R. Buitelaar, T. Nussbaumer, and C. Schönenberger, Phys. Rev. Lett. **89**, 256801 (2002).
[11] J. Rammer and H. Smith, Rev. Mod. Phys. **58**, 323 (1986).
[12] The measured gap 2Δ is smaller than the bulk value of Al (0.36 meV), which is attributed to the intermediate Au layer, necessary to obtain good electrical contact between the leads and the MWNT.
[13] The saturation of the Kondo resonance of Fig. 1 close to $2e^2/h$ suggests that the tunneling rates of both junctions are quite similar.
[14] E. Scheer *et al.*, Phys. Rev. Lett. **78**, 3535 (1997).
[15] G. Johansson, V. S. Shumeiko, E. N. Bratus, and G. Wendin, Physica (Amsterdam) **293C**, 77 (1997).
[16] E. Scheer *et al.*, Phys. Rev. Lett. **86**, 284 (2001).